13th International Symposium on Turbulence and Shear Flow Phenomena (TSFP13)
Montreal, Canada, June 25–28, 2024

INDOOR-OUTDOOR POLLUTANT EXCHANGE IN A FLOW THROUGH A HOLLOW CUBE IMMERSED IN A TURBULENT BOUNDARY LAYER

Subhajit Biswas
Department of Aeronautics and Astronautics
University of Southampton
Southampton, SO16 7QF, United Kingdom
s.biswas@soton.ac.uk

Christina Vanderwel
Department of Aeronautics and Astronautics
University of Southampton
Southampton, SO16 7QF, United Kingdom
C.M.Vanderwel@soton.ac.uk

ABSTRACT

Understanding how turbulent processes disperse air pollution inside buildings is crucial for urban planning and occupancy comfort. Driven by this motivation, the present work investigates an idealization of the indoor-outdoor exchange of a passive scalar pollutant in an urban environment, namely, flow-through an isolated hollow cube, a scaled-down (about 40:1) model building immersed in a turbulent boundary layer, with windows in the upstream and downstream faces of the cube. Presently, two cases are investigated where the first one involves an indoor ground-level passive scalar source, and the second one has an outdoor ground-level source placed upstream to the model, with both being studied for a fixed Reynolds number (Re=$U_{Ref}H/\nu$) of ≈20,000; here U_{Ref} is the incoming flow velocity at the cube height (H) measured without the cube. The experiments take place in a recirculating water tunnel where Planar Laser-induced Fluorescence (PLIF) measurements are performed to capture the mean and transient behaviours of a scalar and Particle Image Velocimetry (PIV) to capture the velocity fields, with these two being performed simultaneously. Changing the source position significantly alters the scalar transport and distribution inside the model. The indoor injection case shows scalar accumulation in re-circulation flow regions near the top and bottom walls inside the cube, while in the outdoor case, a relatively uniform scalar buildup within the cube is observed. These differences are found to be due to the distinction between the two cases in the advective and turbulent scalar transport mechanisms. The insights from the present results can significantly contribute to our understanding and modelling of pollutant(s) exchange between indoor and outdoor environments in intricate atmospheric boundary layer conditions.

INTRODUCTION

In urban environments, pollutants originate from both indoor and outdoor sources, posing a threat to human health (Hanna, 2003; Blake & Wentworth, 2023; Mulcahy, 2023). Numerous studies focused on understanding flow patterns and the spread of pollutants in both outdoor settings (Robins, 2003; Meroney, 2004; Li *et al.*, 2006; Tominaga & Stathopoulos, 2013; Blocken *et al.*, 2013; Lim *et al.*, 2022) and indoor spaces (Holmberg & Li, 1998; Zhang & Chen, 2006). The outdoor dispersion studies have ranged from simple configurations, such as the flow and dispersion over a simple cube (Oke *et al.*, 2017; Wang *et al.*, 2006), to more intricate scenarios involving the flows over an array of cubes (Vanderwel & Ganapathisubramani, 2019) and realistic clusters of buildings (Lim *et al.*, 2022; Xie *et al.*, 2008). Additionally, significant efforts have been directed towards comprehending flow patterns and dispersion within indoor environments (Lim *et al.*, 2024; González-Martín *et al.*, 2021; Posner *et al.*, 2003; Ai & Mak, 2016). However, the existing body of literature exhibits a noticeable absence of investigations into cross-ventilation coupled with indoor and/or outdoor dispersion sources. To address this gap, the present work experimentally investigates an idealization of a cross-ventilating flow through a model building, namely, flow through a hollow cube with two ground-level pollutant sources, with the first one being inside the cube (case **A**) and the second one placed outside (case **B**) upstream of the model, with these two cases being studied separately. Presently, simultaneous Planar Laser-Induced Fluorescence (PLIF) and Particle Image Velocimetry (PIV) measurements are employed to characterize the indoor-outdoor transport of the scalar.

A large number of studies emphasised the critical role of cross ventilation for ensuring a healthy indoor environment (Finnegan *et al.*, 1984; Van Hooff & Blocken, 2010). A few recent studies reported flow through a hollow building under atmospheric boundary layer conditions. For instance, Kosutova *et al.* (2019) conducted a study involving airflow through a cuboid-shaped building. They reported the flow characteristics inside the building for various window placements relative to the building's floor. Along similar lines, some qualitative measurements of the indoor scalar concentration were reported by Tominaga & Blocken (2016). However, it is worth noting that these studies, while valuable in shedding light on the flow patterns and turbulence statistics, notably lack simultaneous measurements of both the flow field and scalar quantities, which is crucial for quantifying indoor-to-outdoor scalar transport. To

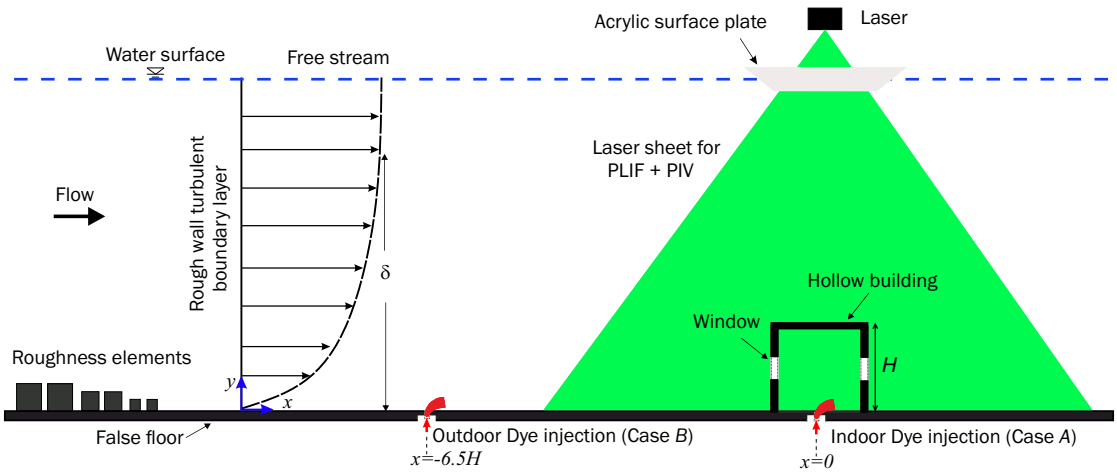

Figure 1. The experimental setup employed in this study is illustrated in the diagram. A hollow cube representing a model building was placed on a false floor assembly, which was affixed to the glass floor within the flume test section. The cube faced the incoming rough-wall boundary layer generated by a series of roughness blocks mounted on the false floor upstream of the test section. Individual scalar (dye) sources were implanted on the building's floor, both inside and upstream of the model. Simultaneous measurements using Planar Laser-Induced Fluorescence (PLIF) and Particle Image Velocimetry (PIV) were performed in the stream-wise centre plane (x-y plane), passing along the building centre and the source. The dye injection took place through a 5 mm orifice flush-mounted at the centre of the model (x=0, in case **A**) and upstream to the model (x=-6.5H, in case **B**), as highlighted in red.

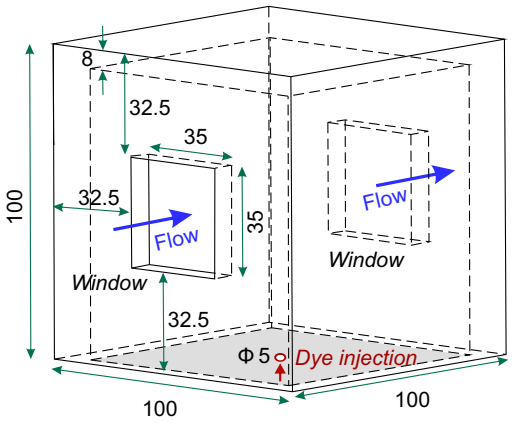

Figure 2. Schematic depicting the three-dimensional view of the hollow building model employed in the present study. All dimensions are presented in millimetres.

bridge this gap, the present work investigates flow through a hollow cube submerged inside a rough-wall turbulent boundary layer, with simultaneous PLIF and PIV measurements capturing both the velocity and concentration fields. This paper presents an analysis of simultaneous flow and dispersion processes for a cross-ventilated generic building configuration.

EXPERIMENTAL METHODOLOGY

Building model

The model building is a transparent acrylic cube with a height (H) of 100 mm and a wall thickness of 8 mm, as illustrated in Fig. 2. The cube features two opposing openings (windows) on the windward and leeward facades, each measuring 35 mm × 35 mm, resulting in a facade porosity of approximately 10%, resembling the configuration used by Kosutova *et al.* (2019). The scale of the model, relative to a typical single-storey building in the UK, ranges from 30:1 to 45:1, consistent with prior research (Lim *et al.*, 2024; Richards *et al.*, 2007). In the indoor-injection case (case **A**), the passive scalar (Rhodamine 6G dye) was injected from the centre of the bottom floor of the building, as depicted in Fig. 1, while in the outdoor case (case **B**), the dye was injected 6.5H upstream to the model's centre (x=0). Despite the same flow conditions in **A** and **B**, substantial variations in scalar transport and distribution within the model were observed due to the altered positions of the scalar source, as will be discussed.

Water tunnel setup

The experiments were performed inside the Recirculating Water Tunnel (RWT) facility at the University of Southampton's Boldrewood Campus, having a test section of 8.1 m in length, 1.2 m in width and 0.9 m in height. The water depth was maintained at 0.6 m throughout the experiments. The hollow cube was mounted on the false floor placed on the test section's glass floor. The condition of an atmospheric turbulent boundary layer was obtained using a series of roughness blocks placed upstream as shown in Fig. 1 (for details, see Lim *et al.* (2022)). Throughout all the experiments, the freestream velocity was kept fixed at 0.25 m/s with the corresponding building Reynolds number being about 20,000; here, $Re = U_{Ref}H/\nu$, where U_{Ref} is the streamwise velocity at building height, H, measured in the absence of the building. The present Re is kept larger than the critical Reynolds number threshold of about 5000-10,000 (for buildings) to ensure Reynolds number independence and thus will reproduce the turbulence characteristics of a full-scale flow (Plate, 1999).

Scalar and velocity measurements

The two-dimensional maps of the velocity (U) and the scalar concentration (C), within and outside the building, were captured simultaneously through Particle Image Velocimetry (PIV) and Planar Laser-Induced Fluorescence (PLIF), respectively, in the streamwise plane (x-y) along the centreline of the building and also aligned with the source location, as shown in Fig. 1. The experimental setup facilitated the injection of a neutrally buoyant solution of Rhodamine 6G fluorescent dye at the floor within the cube and upstream to the cube, essentially

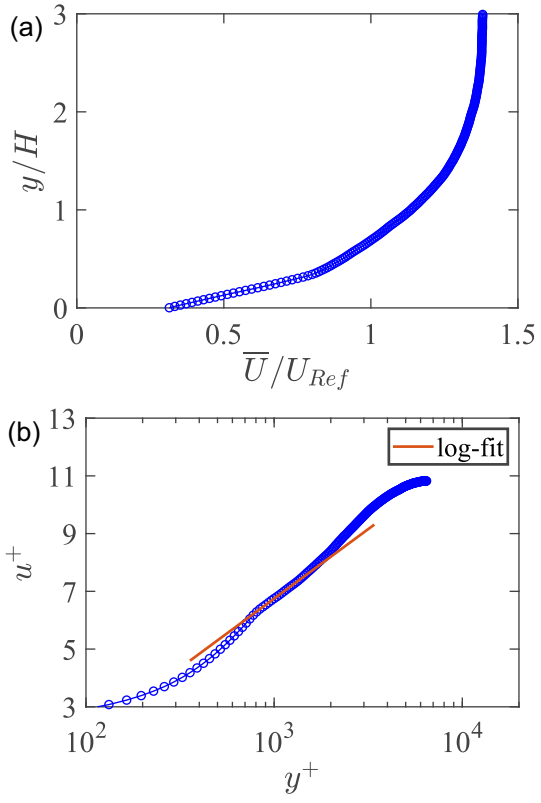

Figure 3. Characterization of the incoming flow at Re of 20,000, is shown in terms of the: (a) normalized mean stream-wise velocity ($\overline{U}/U_{Ref}$) along the wall-normal direction (y/H), and (b) mean stream-wise velocity in linear-logarithmic scale (u^+ vs. y^+). These base flow measurements were taken in the water tunnel test section without the cube.

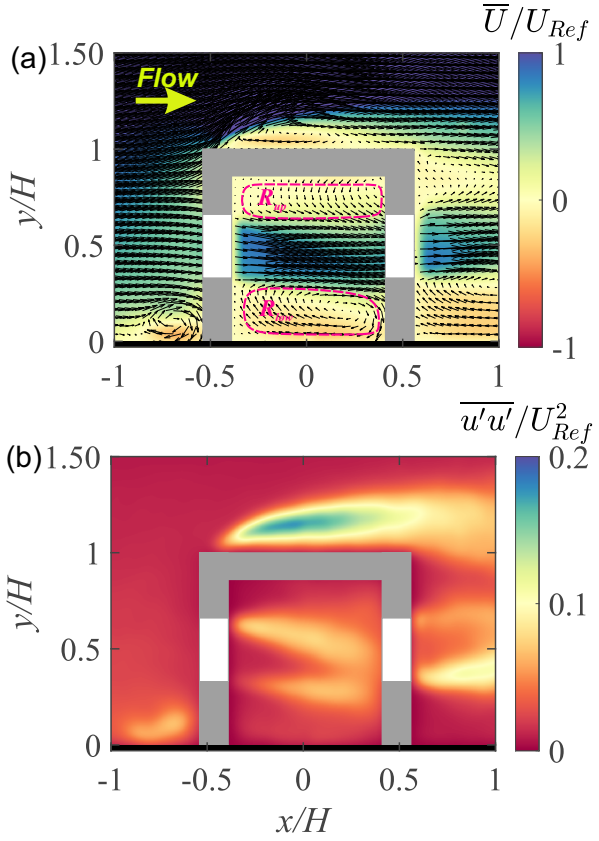

Figure 4. Time averaged (a) vector map overlaid with streamwise velocity ($\overline{U}/U_{Ref}$), and (b) in-plane streamwise component of turbulent kinetic energy ($\overline{u'u'}/U^2_{Ref}$), at Re of 20,000.

replicating ground-level point sources of a passive scalar with negligible effects on the flow (see Lim & Vanderwel (2023)). The aqueous solution of the dye had concentrations (C_S) of 1 mg/L and 100 mg/L, for cases **A** and **B**, respectively, and was injected at a constant flow rate of (Q_{dye}) of 7 mL min^{-1} through a thin tube connected to the building floor (see Fig. 1). The higher C_S in **B** was chosen to ensure a better signal-to-noise ratio downstream where the model is positioned. The local dye concentration (C) was determined from the fluorescence intensity following a calibration procedure, and the details can be found in the recent study by Lim *et al.* (2022). The dye Schmidt number was 2500±300, indicating a much higher momentum diffusion rate than the scalar diffusion rate (Vanderwel & Tavoularis, 2014).

For PIV measurements, the flow was seeded with 50 μm polyamide particles. In both PIV and PLIF, a 100 mJ Nd:YAG double-pulsed laser with a 532 nm emission wavelength provided illumination. Two cameras were equipped with appropriate filters to distinguish PIV and PLIF signals. The PIV post-processing utilized LaVision DaVis 10 software, while in-house codes were employed for PLIF post-processing (Lim & Vanderwel, 2023). The flow field, illuminated at 10 Hz, was captured at a spatial resolution of 0.18 mm/pixel. To ensure the convergence of time-averaged statistics, 2000 pairs of images were processed in DaVis 10. A 4-pass interrogation window, ranging from 128×128 to 24×24 with a 50% overlap, was employed to maintain a high correlation (see Lim & Vanderwel (2023) for additional PIV processing details). The simultaneously measured velocity and concentration fields were integrated into a unified coordinate system, enabling the calculation of joint velocity-concentration statistics. The measurement uncertainty for these joint statistics was kept below 10%.

Boundary layer characterization

Before beginning experiments involving the cube, the incoming boundary layer was characterized without the model in the test section. In figure 3, the wall-normal (y/H) profile of the mean stream-wise velocity ($\overline{U}/U_{Ref}$), and velocity profile in linear-logarithmic scale (u^+ vs. y^+), are shown; here, $\overline{U}$ is the mean stream-wise velocity, u^+ is calculated as $\overline{U}/u_\tau$, and y^+ is the wall-normal co-ordinate in logarithmic scale= yu_τ/ν. The boundary layer thickness (δ) based on the $0.99U_\infty$ cut-off for U was about 200 mm. The friction velocity (u_τ) was estimated following the total stress method from the square root of the peak of the Reynolds shear stress (Walker, 2014). It can be noted that the friction Reynolds number, defined here as $Re_\tau = u_\tau\delta/\nu$, was about 4600.

RESULTS AND DISCUSSIONS

Velocity field

Turbulent flows around geometric structures such as cubes are characterized by phenomena like separation, re-circulation, and vortex shedding. Introducing openings in such configurations results in an internal flow that is unsteady in nature. In the present configuration, the internal flow involves a jet penetrating the cube and two re-circulation regions (R_{up}, R_{low}) adjacent to the upper and lower walls, as delineated by dashed (in magenta) closed contours in Fig. 4(a). Outside the cube, we observe re-circulation regions, with the first one be-

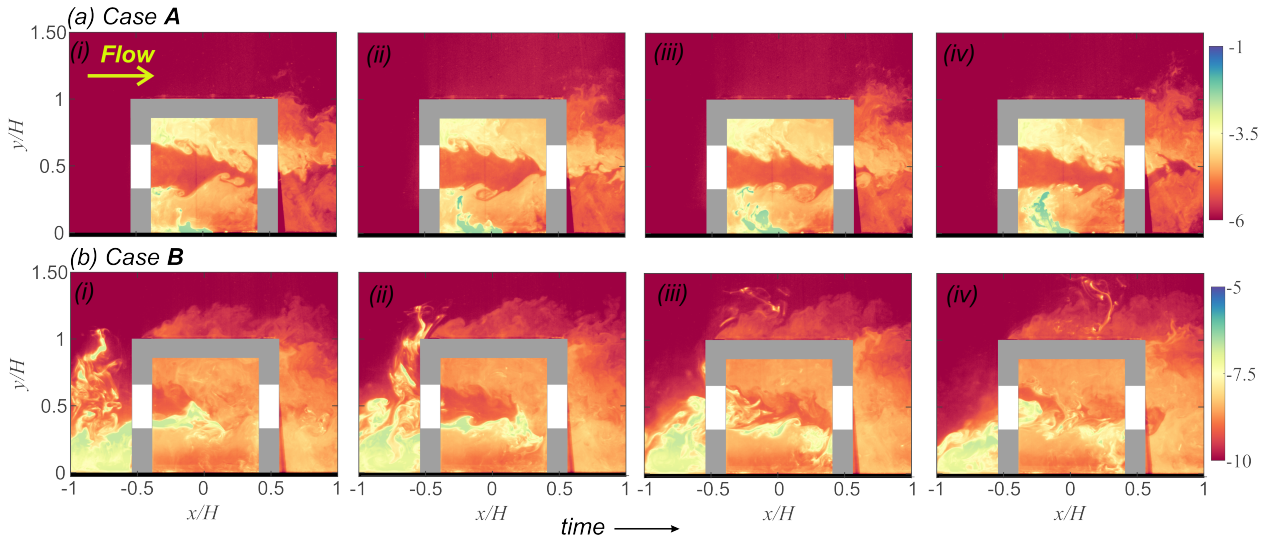

Figure 5. Instantaneous scalar fields (C) normalised by the source concentration (C_S), shown at Re of 20,000, for (a) indoor (case **A**) and (b) outdoor (case **B**) injection cases. These instantaneous scalar fields are shown at an interval of 0.2 s.

ing near-ground upstream to the cube and the other one on the rooftop. The instantaneous velocity fields inside the cube, although not depicted here, reveal the jet's flapping behaviour. Such dynamic phenomena carry significant implications for scalar transport within the cube, as will be discussed. Alongside the mean advective flow, also depicted in Fig. 4(b) is the in-plane streamwise component of the turbulent kinetic energy ($\overline{u'u'}/U^2_{Ref}$) which within the cube, seems to be dominant at the interface of the jet and reverse flow regions. These broad flow characteristics are in line with previous studies (Kosutova *et al.*, 2019; Tominaga & Blocken, 2016) on cross-ventilating flows through genetic building configurations.

Scalar field

The dynamic nature of the flow within the cube is also reflected in the side-view instantaneous scalar fields presented in Fig. 5, shown for both indoor (**A**) and outdoor (**B**) injection cases, indicating the unsteadiness in the indoor flow. It is worth highlighting that while the flow field remains invariant between cases **A** and **B**, significant disparities in scalar transport mechanisms are observed, as also evident from both the instantaneous concentration maps (C/C_S) in Figs. 5(a,b), and the time-averaged concentration ($\overline{C}/C_S$) and variance ($\overline{c'^2}/C_S^2$) in Figs. 6(a,b); here, the instantaneous concentration fluctuation (c') is defined as $c' = C - \overline{C}$. Throughout this manuscript, the scalar concentration (C) is normalized by the source strength (C_S), in accordance with prior studies (Lim *et al.*, 2022; Lim & Vanderwel, 2023). It is also pertinent to note that the concentration fields (images) were acquired once the flow through the cube and the concentration within it had reached a statistically steady state in a mean (over time) sense.

Moving forward, we now discuss the differences in the scalar distribution and transport between the indoor (**A**) and outdoor (**B**) injection cases. The instantaneous scalar fields in Fig. 5 show that in **A**, there is pronounced scalar accumulation in the re-circulation regions near the top and bottom walls of the cube, with notably higher scalar intensity near the bottom wall, as also evident from the time-averaged scalar concentration ($\overline{C}/C_S$) in Fig. 6(a(i)). The side-view time-series scalar maps illustrate that the scalar introduced near the source is transported towards the upstream wall (along the negative x direction) via the reverse flow within the lower re-circulation region (R_{low}, Fig. 4(a)). Subsequently, some of the transported scalar is carried along the positive y direction and then transported downstream towards the positive x direction. Following this, a part of the scalar is accumulated within R_{low}, while the remaining is transported into the jet. While the scalar trapped within the jet is carried downstream, a portion of the scalar is observed to be transported into both the upper (R_{up}) and lower (R_{low}) re-circulation regions. This phenomenon could be attributed to the vertically oscillating nature of the jet, and the presence of instability at the interface between the jet and R_{up} and R_{low}, as evidenced by the formation of interfacial structures, for instance, in Fig. 5(a(i)). Following these processes, the scalar remaining within the jet, is flushed out of the cube, while the rest accumulates in the upper and lower re-circulation regions.

In case **B**, the stream of scalar upstream to the cube, while approaching towards it, a fraction of the scalar would bypass via around and over the cube, and the remaining will be transported through the cube. The side view instantaneous scalar fields show that the incoming scalar enters the cube mostly intermittently in the form of scalar parcels/patches. The parcel of the scalar within the jet, while passing through the cube, a fraction of the scalar gets transported into R_{up} and R_{low}. The side views of the instantaneous velocity and scalar fields show that the oscillating nature of the jet and the development of the interfacial instability between the jet and the re-circulation regions promote the exchange of the scalar between the jet and the re-circulation regions, similar to the case **A**. It may be noted that since the lower part of the jet is seen to contain a relatively larger portion of the scalar, for instance, in Fig. 5(b(i))), this would result in a relatively larger concentration in the lower half of the cube, which is also evident from the mean concentration ($\overline{C}/C_S$) shown in Fig. 6(a(ii)). However, in comparison with case **A**, the time-averaged indoor concentration ($\overline{C}/C_S$) is relatively uniform, indicating a comparatively well-mixing in **B**. Following the mean concentration, the scalar variance in Fig. 6(b(ii)) is found to be more prominent within the jet and is relatively weaker within the re-circulation regions, which is notably different from **A** (in Fig. 6(b(i))).

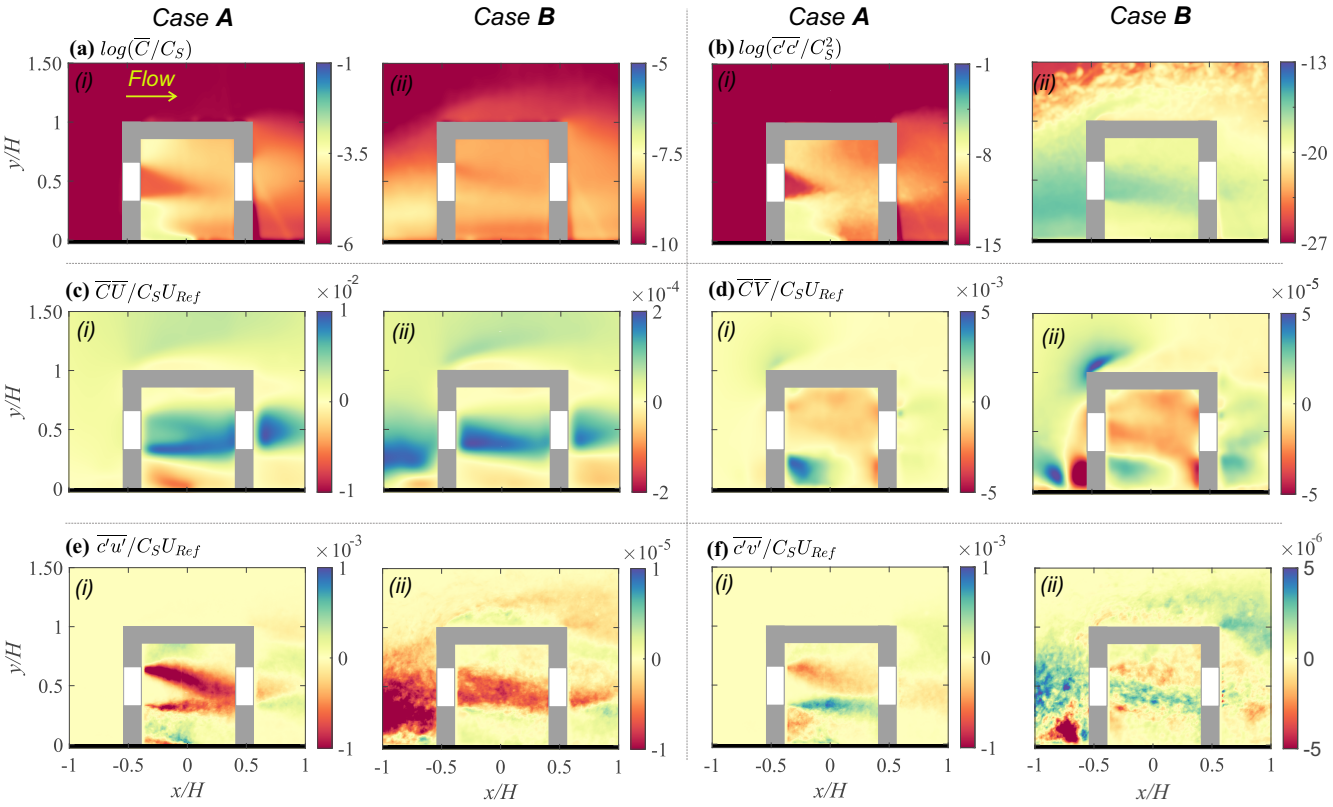

Figure 6. The time-averaged normalised: (a) scalar concentration ($\overline{C}/C_S$, in *log* scale), (b) concentration variance ($\overline{c'^2}/C_S^2$, in *log* scale), (c) stream-wise advective flux ($\overline{C}\,\overline{U}/C_S U_{Ref}$), (d) wall-normal advective flux ($\overline{C}\,\overline{V}/C_S U_{Ref}$), (e) streamwise turbulent flux ($\overline{c'u'}/C_S U_{Ref}$), and (f) wall-normal turbulent flux ($\overline{c'v'}/C_S U_{Ref}$), all shown at Re≈20,000, for indoor (Fig. (i), case **A**) and outdoor (Fig. (ii), case **B**) injections.

Advective and turbulent flux

To further understand the scalar distribution within the cube, we delve into the mechanisms of scalar transport by examining both the advective ($\overline{C}\,\overline{U}/C_S U_{Ref}$, $\overline{C}\,\overline{V}/C_S U_{Ref}$) and turbulent fluxes ($\overline{c'u'}/C_S U_{Ref}$, $\overline{c'v'}/C_S U_{Ref}$), for both streamwise and wall-normal components. The advective fluxes are obtained from the product of the time-averaged scalar concentration ($\overline{C}$) with the mean streamwise velocity field ($\overline{U}$) and wall-normal velocity ($\overline{V}$). On the other hand, the turbulent fluxes are obtained from the time-averaging of the product of the instantaneous scalar fluctuation (c') with the instantaneous streamwise (u') and wall-normal (v') velocity fluctuations.

Beginning with case **A**, in Fig. 6(c(i)), we notice in close proximity to the source a negative streamwise advective flux ($\overline{C}\,\overline{U}/C_S U_{Ref}$), transporting the injected scalar towards the upstream wall. This results in a localized concentration peak around the left-most ground-level corner of the cube, as already observed in Fig. 6(a(i)). Simultaneously, from the corner area, a positive $\overline{C}\,\overline{V}/C_S U_{Ref}$ transports the scalar upward towards the jet. The jet exhibits a relatively stronger positive $\overline{C}\,\overline{U}/C_S U_{Ref}$, facilitating outward scalar transport from the cube.

In contrast to the advective fluxes, the turbulent scalar fluxes in Figs. 6(e(i), f(i)) appear strongest around the interface of the jet and re-circulation flow regions. The streamwise component ($\overline{c'u'}/C_S U_{Ref}$) is predominantly negative, indicating its role in scalar transport opposite to the streamwise direction. Conversely, the positive and negative wall-normal fluxes ($\overline{c'v'}/C_S U_{Ref}$) in R_{low} and R_{up}, respectively, suggest scalar transport (and mixing) from the re-circulation regions into the jet. In case **B**, the streamwise advective flux ($\overline{C}\,\overline{U}/C_S U_{Ref}$) is found to be prominent only within the jet, as seen in Fig. 6(c(ii)), similar to **A**, which would be expected due to the higher streamwise velocity. However, unlike **A**, the streamwise turbulent scalar fluxes ($\overline{c'u'}/C_S U_{Ref}$) in Fig. 6(e(ii)) appear strongest within the jet, promoting mixedness within the jet. On the other hand, the spatial variations of the wall-normal turbulent flux ($\overline{c'v'}/C_S U_{Ref}$) in Fig. 6(f(ii)) indicates its role in scalar mixing in both within the jet and the re-circulation regions.

CONCLUSIONS

The present work experimentally investigated a cross-ventilating flow through a hollow cube, with ground-level passive scalar sources inside and outside the cube, immersed in a rough-wall turbulent (water) boundary layer. The primary focus was on characterizing the scalar transport within the cube and toward the outdoors through simultaneous measurements of the scalar and the flow, using Planar Laser-Induced Fluorescence (PLIF) and Particle Image Velocimetry (PIV), respectively.

Dramatic differences in the scalar transport and distribution were observed between the indoor and outdoor injection cases instead of the flow patterns being the same. Concerning scalar distribution, the indoor injection exhibited scalar accumulation in re-circulation regions near the top and bottom walls, with the peak concentration being around the source and the upstream near-ground corner. Additionally, non-uniform scalar concentration was noticeable in the lower part of the cube. In comparison, the outdoor injection case resulted in a relatively uniform scalar buildup within the cube, indicating a

better mixing compared to the indoor injection. These overall observations will provide valuable insights into the characterization of the indoor-outdoor pollutant exchange in a cross-ventilating scenario.

In connection with the present findings, several prospects for potential future investigation remain open:

- Finding a suitable normalization of the scalar concentration would ensure a more sensible quantitative comparison of the scalar concentration and the fluxes across the indoor and outdoor injection cases.
- Using the present results to inform the boundary conditions of existing urban dispersion models could improve the accuracy of predictions of pollutant concentrations in indoor and outdoor environments.
- The present observations assume an Eulerian framework; however, adapting a Lagrangian approach could help further understand the important spatio-temporal characteristics of scalar transport.
- The current experiments using PLIF and PIV have helped reveal the spatial maps of the scalar in a simple geometry; this could help inform future water tunnel and wind tunnel studies exploring other parameters and more complex geometries.

In a nutshell, the present study holds substantial potential in enhancing our understanding and modelling of pollutant exchange between indoor and outdoor environments in complex atmospheric boundary layer conditions.

REFERENCES

Ai, ZT & Mak, Cheuk Ming 2016 Large eddy simulation of wind-induced interunit dispersion around multistory buildings. *Indoor Air* **26** (2), 259–273.

Blake, E & Wentworth, J 2023 Urban outdoor air quality. *UK Parliament Post* .

Blocken, B, Tominaga, Y & Stathopoulos, T 2013 CFD simulation of micro-scale pollutant dispersion in the built environment. *Building and Environment* **64**, 225–230.

Finnegan, MJ, Pickering, CA & Burge, PS 1984 The sick building syndrome: prevalence studies. *British medical journal (Clinical research ed.)* **289** (6458), 1573.

González-Martín, J, Kraakman, N J R, Pérez, C, Lebrero, R & Muñoz, R 2021 A state–of–the-art review on indoor air pollution and strategies for indoor air pollution control. *Chemosphere* **262**, 128376.

Hanna, S 2003 Flow and dispersion in urban areas. *Annu. Rev. Fluid Mech.* **35**, 469–496.

Holmberg, S & Li, Y 1998 Modelling of the indoor environment–particle dispersion and deposition. *Indoor air* **8** (2), 113–122.

Kosutova, K, van Hooff, T, Vanderwel, C, Blocken, B & Hensen, J 2019 Cross-ventilation in a generic isolated building equipped with louvers: Wind-tunnel experiments and cfd simulations. *Building and Environment* **154**, 263–280.

Li, X-X, Liu, C-H, Leung, DYC & Lam, K M 2006 Recent progress in cfd modelling of wind field and pollutant transport in street canyons. *Atmospheric Environment* **40** (29), 5640–5658.

Lim, H.D., Foat, T. G., Parker, S. T. & Vanderwel, C. 2024 Experimental investigation of scalar dispersion in indoor spaces. *Building and Environment* p. 111167.

Lim, HD, Hertwig, D, Grylls, T, Gough, H, van Reeuwijk, M, Grimmond, S & Vanderwel, C 2022 Pollutant dispersion by tall buildings: laboratory experiments and large-eddy simulation. *Experiments in Fluids* **63** (6), 92.

Lim, HD & Vanderwel, C 2023 Turbulent dispersion of a passive scalar in a smooth-wall turbulent boundary layer. *Journal of Fluid Mechanics* **969**, A26.

Meroney, RN 2004 Wind tunnel and numerical simulation of pollution dispersion: a hybrid approach. *Paper for Invited Lecture at the Croucher Advanced Study Institute, Hong Kong University of Science and Technology* pp. 6–10.

Mulcahy, E 2023 A bill before parliament for the right to breath clean air. *BMJ: British Medical Journal (Online)* **380**, p224.

Oke, TR, Mills, G, Christen, A & Voogt, JA 2017 *Urban Climates*. Urban Climates, 1st ed., Cambridge University Press.

Plate, E J 1999 Methods of investigating urban wind fields—physical models. *Atmospheric Environment* **33** (24-25), 3981–3989.

Posner, JD, Buchanan, CR & Dunn-Rankin, D_ 2003 Measurement and prediction of indoor air flow in a model room. *Energy and buildings* **35** (5), 515–526.

Richards, PJ, Hoxey, RP, Connell, BD & Lander, DP 2007 Wind-tunnel modelling of the silsoe cube. *Journal of Wind Engineering and Industrial Aerodynamics* **95** (9-11), 1384–1399.

Robins, A 2003 Wind tunnel dispersion modelling some recent and not so recent achievements. *Journal of wind engineering and Industrial Aerodynamics* **91** (12-15), 1777–1790.

Tominaga, Y & Blocken, B 2016 Wind tunnel analysis of flow and dispersion in cross-ventilated isolated buildings: Impact of opening positions. *Journal of Wind Engineering and Industrial Aerodynamics* **155**, 74–88.

Tominaga, Y & Stathopoulos, T 2013 CFD simulation of near-field pollutant dispersion in the urban environment: A review of current modeling techniques. *Atmospheric Environment* **79**, 716–730.

Van Hooff, T & Blocken, B 2010 Coupled urban wind flow and indoor natural ventilation modelling on a high-resolution grid: A case study for the amsterdam arena stadium. *Environmental Modelling & Software* **25** (1), 51–65.

Vanderwel, C & Ganapathisubramani, B 2019 Turbulent boundary layers over multiscale rough patches. *Boundary-Layer Meteorology* **172**, 1–16.

Vanderwel, C & Tavoularis, S 2014 Measurements of turbulent diffusion in uniformly sheared flow. *Journal of fluid mechanics* **754**, 488–514.

Walker, J M 2014 The application of wall similarity techniques to determine wall shear velocity in smooth and rough wall turbulent boundary layers. *Journal of Fluids Engineering* **136** (5), 051204.

Wang, Harold F, Zhou, Yu, Chan, CK & Lam, Ka Se 2006 Effect of initial conditions on interaction between a boundary layer and a wall-mounted finite-length-cylinder wake. *Physics of Fluids* **18** (6).

Xie, Z-T, Coceal, O & Castro, I P 2008 Large-eddy simulation of flows over random urban-like obstacles. *Boundary-layer meteorology* **129**, 1–23.

Zhang, Z & Chen, Q 2006 Experimental measurements and numerical simulations of particle transport and distribution in ventilated rooms. *Atmospheric environment* **40** (18), 3396–3408.